

Temporal change of geologic features in the pyroclastic surge dominated deposits of the Komakusadaira pyroclastics in Zao volcano, NE Japan

Y. Takebe, and M. Ban

ban@sci.kj.yamagata-u.ac.jp

Abstract— The Zao volcano in northeast Japan is one of representative stratovolcanoes having a crater lake in the summit area. We studied geologic features of the pyroclastic surge dominated deposits of the Komakusadaira pyroclastics, which is the thickest unit of the youngest stage (ca. 33 ka–present) and revealed the temporal change of the type of eruption. We also examined the petrographic features of the products along with the stratigraphy.

The pyroclastics are composed of 27 layers by five facies; scoriaceous tuff, lapilli tuff, agglutinate, volcanic breccia, and tuff breccia. By unconformities, seven episodes are recognized, which are grouped to three periods of episode 1, episodes 2–4 and episodes 5–7, because time gaps within episodes 2–4, and 5–7 are short. The ages of these periods are estimated to be ca. 32–33, 31, and 27 kyr BP. The tuff breccia, volcanic breccia–agglutinate, and scoriaceous tuff facieses are characterizing the three periods respectively. The phreatic to phreatomagmatic eruptions with minor amount of juvenile fragments would be occurred repeatedly in the first period. During the second period, the eruption type had changed from the vulcanian to the phreatomagmatic, which formed pyroclastic surge with abundant spatter and ballistic bombs. The phreatomagmatic eruptions would continue to the late part of this period, but the explosivity would decrease. In the third period, the type of the eruption is mainly the phreatomagmatic, but the explosivity of the activity would be much smaller than that of the former period.

All rocks are olv-cpx-opx basaltic andesite to andesite. The petrographic features are different among three periods. Mostly, mafic minerals are of simple zoning type and plagioclases are patchy and oscillatory zoning type in the first period. In contrast, complex zoning pyroxenes and honeycomb texture plagioclase with larger glass inclusions are remarkable in the second period. In the third period, olivine phenocrysts are abundant and honeycomb texture plagioclase with smaller glass inclusions is characteristically observed. These distinct features for each period would reflect the differences in magma system in each period.

Keywords— pyroclastic surge, scoriaceous tuff, agglutinate, Zao volcano in Japan

I. INTRODUCTION

THE pyroclastic surge (base surge) are commonly associated with formation of maar type small volcanoes, and also andesitic stratovolcanoes with crater lakes [1]. In the later cases, the pyroclastic surge phenomena are frequently reported [2]–[3],

but studies on the pyroclastic surge dominated successions by repeated eruptions of mainly phreato or phreatomagmatic and associated other types have not been sufficiently performed, because establishing the detailed volcanic stratigraphy is usually very hard by the difficulties of the approach to outcrops, finding the outcrops preserving the successive layers.

The Zao volcano in northeast Japan is one of representative stratovolcanoes having a crater lake in the summit area. In the summit area of the Zao, some of the pyroclastic surge dominated successions are well preserved. Investigation on these deposits will provide information on temporal change of the type of eruption. This information will be very useful to elucidate future volcanic activity. Among the pyroclastic surge dominated successions, we examined the Komakusadaira pyroclastics in the present study. Because the Komakusadaira pyroclastics is the largest during the newest stage of Zao volcano and the pyroclastic successions are very well preserved except for the upper most part. We will also provide the petrographic features of the juvenile fragments and examine the temporal change of these along with the stratigraphy.

II. GEOLOGICAL BACKGROUND

Northeastern Japan is well known as a volcanic arc. Zao volcano is a representative active volcano on the volcanic front (Fig. 1a). Volcanic activity commenced at ca. 1 Ma [4] and has continued to the present day. Geological and petrological studies about the Zao volcano were performed by various authors [4]–[5]. Reference [4] classified the activity of the Zao volcano into four stages based on geologic features (Fig. 1b). Stage 1 products are low-K tholeiitic basalt to basaltic andesite, whereas the products of stages 2–4 are medium-K calc-alkalic basaltic andesite to dacite. Especially, the stage 4 is characterized by the activity of the basaltic andesite magma. The activity of the newest stage proceeded with the formation of the horseshoe-shaped Umanose caldera (ca. 1.7 km diameter) in the summit area at ca. 30 ka [5]. Numerous eruptions have occurred since then. During activity of ca. 2 ka to the present, the pyroclastic cone Mt. Goshikidake was formed in the inner part of Umanose caldera [6]. The newest crater lake Okama is located in the western part of the Goshikidake (Fig. 1c). References [6] and [7] classified the products of stage 4 into

Komakusadaira agglutinate (ca. 33–12.7 ka), Umanose agglutinate (ca. 7.5–4.1 ka), and Goshikidake pyroclastic rock (ca. 2.0–0.4 ka) (Fig. 1c). Komakusadaira agglutinate can be further divided into Komakusadaira pyroclastics, Kumanodake

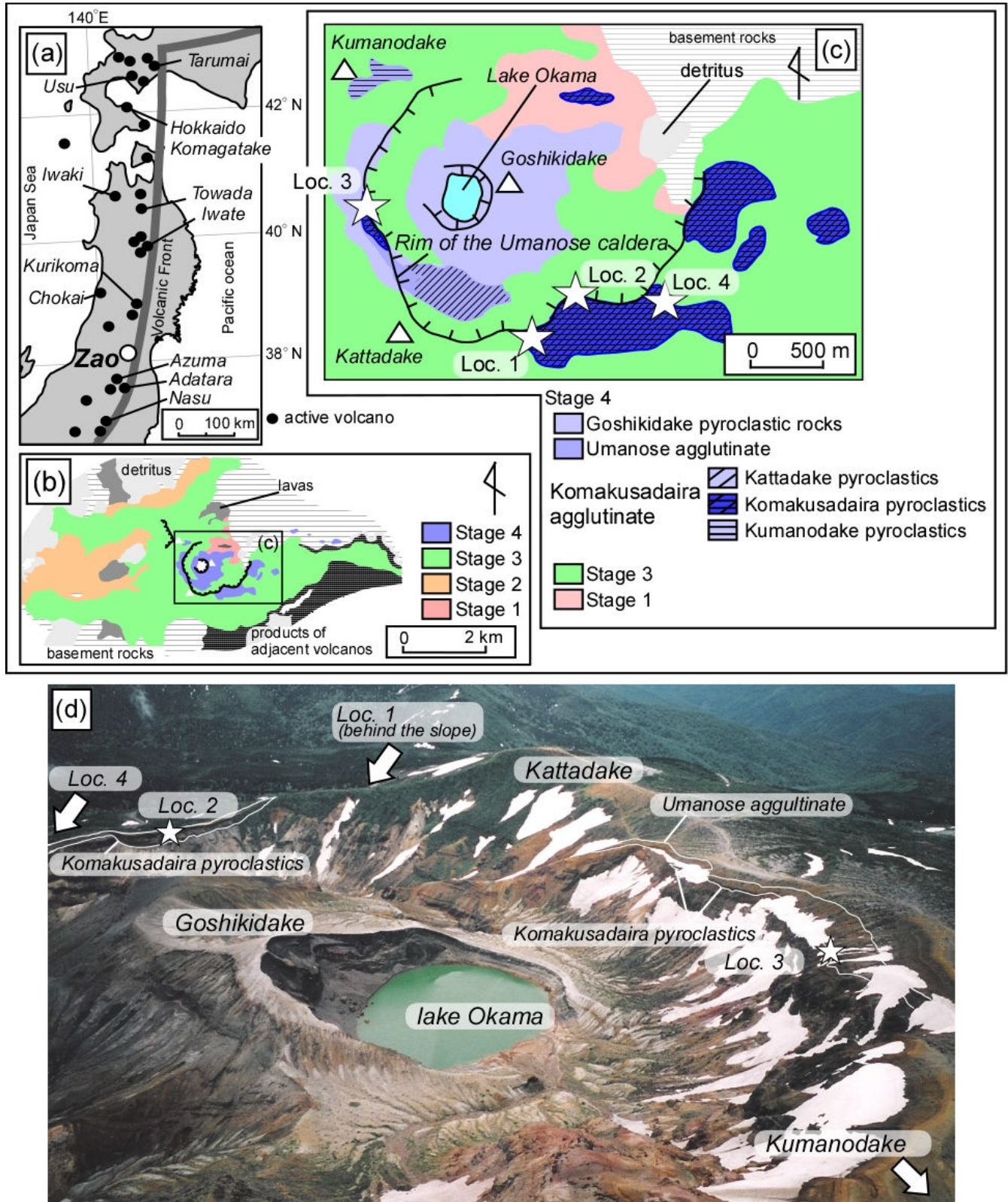


Fig. 1 (a) Location of the Zao volcano in the northeastern Japan. (b) Geological sketch map of the Zao volcano after [5], partly modified. (c) Geological sketch map of the summit area of Zao volcano after [6], partly modified. (d) Air photograph of summit area of the Zao volcano

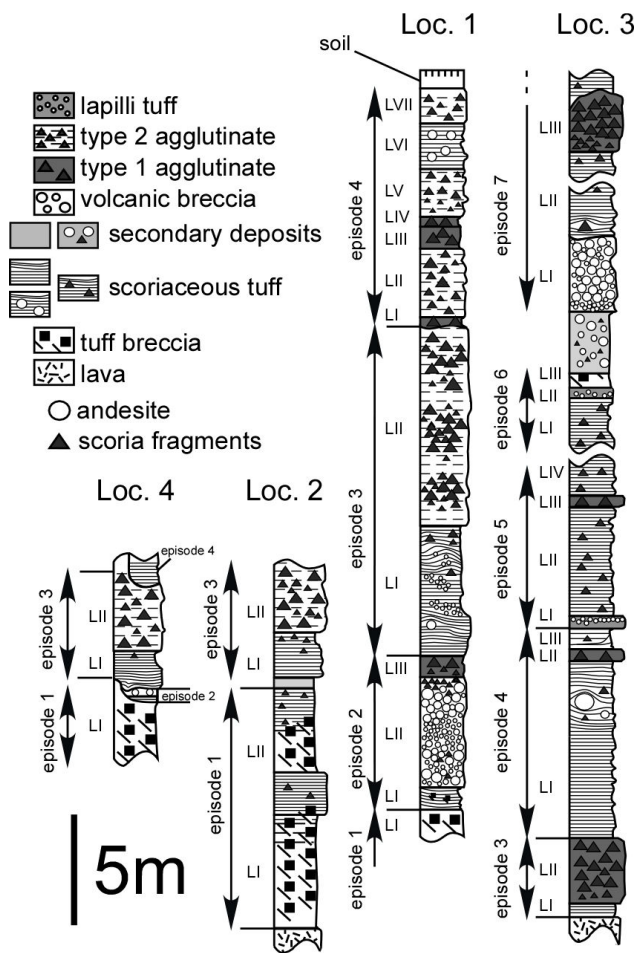


Fig.2 Columnar sections of the well exposed outcrops for the Komakusadaira pyroclastics. L# indicate the number of pyroclastic layer in the ascending order.

agglutinate and Kattadake pyroclastics.

III. FACIES FEATURES

The Komakusadaira pyroclastics are distributed along the top of the Umanose caldera rim (Fig. 1c and d). The products are subdivisible into 27 pyroclastic layers. Seven episodes are defined by unconformities observed in the pyroclastic successions. The products of episodes 1–4 are distributed mainly on the southern to eastern part of the caldera rim, whereas the products of episodes 5–7 are on the western part. The products of episodes 5–7 are exposed only in western part. Representative columnar sections in well exposed four outcrops are shown in Fig. 2. Photographs of these four outcrops are shown in Fig. 3. The pyroclastics composing the Komakusadaira pyroclastics show various facies, such as scoriaceous tuff, lapilli tuff, agglutinate, volcanic breccia, and tuff breccia (Fig. 4). We will describe general features of these facies bellow.

A. Scoriaceous tuff

The scoriaceous tuff facies (Fig. 4a, b, c, d, and e) is the most frequent one of the Komakusadaira pyroclastics. The deposit is

characterized by black to dark gray scoriaceous ash and crystal fragments. The scoriaceous ash is often yellow to reddish brown because of alternation. Many scoriaceous tuff layers contain minor amounts of juvenile scoria fragments (Fig. 4a), glassy andesitic bombs (Fig. 4b), and accessory lithics in varying proportions. The scoria fragments have a black core and weathered yellow crust. These fragments show widely various shapes: they are rounded, fluidal, and cauliflower-shaped. The andesitic bombs are subangular to subrounded, often showing a bread-crust texture. These lithics are up to 1 m, with average of 15–30 cm size. The deposits show unidirectional planar and cross-stratified thin beds (Fig. 4c). A dune structure with altered accessory lithics is often observed (Fig. 4d). Some layers show deformed lapilli-rich lenses (Fig. 4e). Thicknesses of individual thin beds are usually 2–5 cm. The succession of these thin beds comprises one layer of 10 cm to 8 m thickness. The layers show lateral change in thickness. These depositional features suggest a pyroclastic surge origin.

B. Lapilli tuff

The lapilli tuff facies (Fig. 4f and g) is rarely observed intercalating into the scoriaceous tuff sequence as thin massive layer. Thickness of individual lapilli tuff layers is as much as 50 cm. The deposit is characterized by andesitic lapillus with minor amount of black to dark gray scoriaceous ash. Scoriaceous ash often shows weathered yellow to light brown color. The juvenile andesitic lapillus are gray and subangular to subrounded shape. Altered non-juvenile lithics are often observed. The discontinuous lapilli trains are sometimes observed (Fig. 4g). This facies shows no grading such as variation in grain size of lapilli but show weak lamination. These deposition features, especially anomalously sorted without elutriation and weak lamination are compatible with those recognized in near vent deposition of less evolved density currents [1]. Also, discontinuous lapilli trains result from tractional transported of ash and lapilli [8] and [9].

C. Agglutinate

The agglutinate facies is subdivisible into two types. Type 1 is composed mainly of scoria fragments (including spatter) with minor amounts of finer ones (Fig. 4h and i). They are well sorted. The scoria fragments are up to 1 m with an average size of 20–30 cm. They usually have black core and thin reddish oxidized crust although some fragments cores are reddish. These fragments show an elongated and flattened deformation structure, indicating plastic deformation during impact. Thickness of individual layers is 0.2–3 m and laterally continuous. Welding and reverse grading are observed well in cases of thick layers (more than 1 m) (Fig. 4i). Thin layers (less than 1 m) show no grading or welding. These observations suggest that type 1 agglutinate is of strombolian eruption origin.

Type 2 is poorly sorted and is characterized by many scoria fragments (including spatter) in the ash matrix (Fig. 4j). Scoria fragments have a black core and gray or weathered yellow thin crust. These are up to 1 m with an average size of 20–50 cm. Scoria fragments are usually elongated and flattened (Fig. 4j),

although rounded, fluidal, and cauliflower-shaped scoria fragments (less than 30 cm size, Fig. 4j) coexist within the same layer. The matrix consists of a mixture of black scoriaceous ash, crystal fragments, and altered yellow scoriaceous ash. The matrix usually shows weak lamination (Fig. 4j). The laminae tend to be discontinued laterally (Fig. 4k). Thickness of individual layers is up to 10 m. The deposits often become thinner laterally. These deposition features are suggestive of explosive pyroclastic surge origin, with abundant spatter and ballistic bombs.

D. Volcanic breccia

The volcanic breccia facies (Figs. 4l and m) shows poorly sorted, clast-supported, and is characterized by abundant lithics in the matrix of altered blown ash. Lithics are mixture of subangular juvenile and accessory dark gray andesite in variable proportion. Juvenile black scoria fragments are occasionally found. These lithics and fragments are up to 30 cm with an average of 10–15 cm size. Normally and reversely grading, recognized by the variation of size of the fragments, are observed (Fig. 4l and m). These depositional features are suggestive of pyroclastic fall deposit by the vulcanian eruption.

E. Tuff breccia

The tuff breccia facies (Fig. 4n) is characterized by abundant lithics in white to yellow clay matrix. Lithics within tuff breccia facies are dominantly altered gray andesites and non-juvenile scoria fragments, with occasional non-altered juvenile scoriaceous andesite blocks as an additional component. These lithics are subangular to subrounded and up to 15 cm size. The sorting is poor and the grading is not observed. Thickness of individual layers is up to 7 m. Weak stratification is recognizable only in thick layer (more than 1 m). Both of the grain and matrix of the layers of tuff breccia facies were hydrothermally altered, although these are interbedded into unaltered pyroclastic layers. These depositional features are suggestive of phreatic or phreatomagmatic explosion origin.

IV. STRATIGRAPHY

A. episode 1

Episode 1 products cover one of the stage 3 lavas [5]. These deposits crops out at the locations 1, 2, and 4 on the southern to eastern part of top of the caldera rim (Fig. 1). The episode 1 products are best exposed at location 2 (Fig. 3c). At this locality,

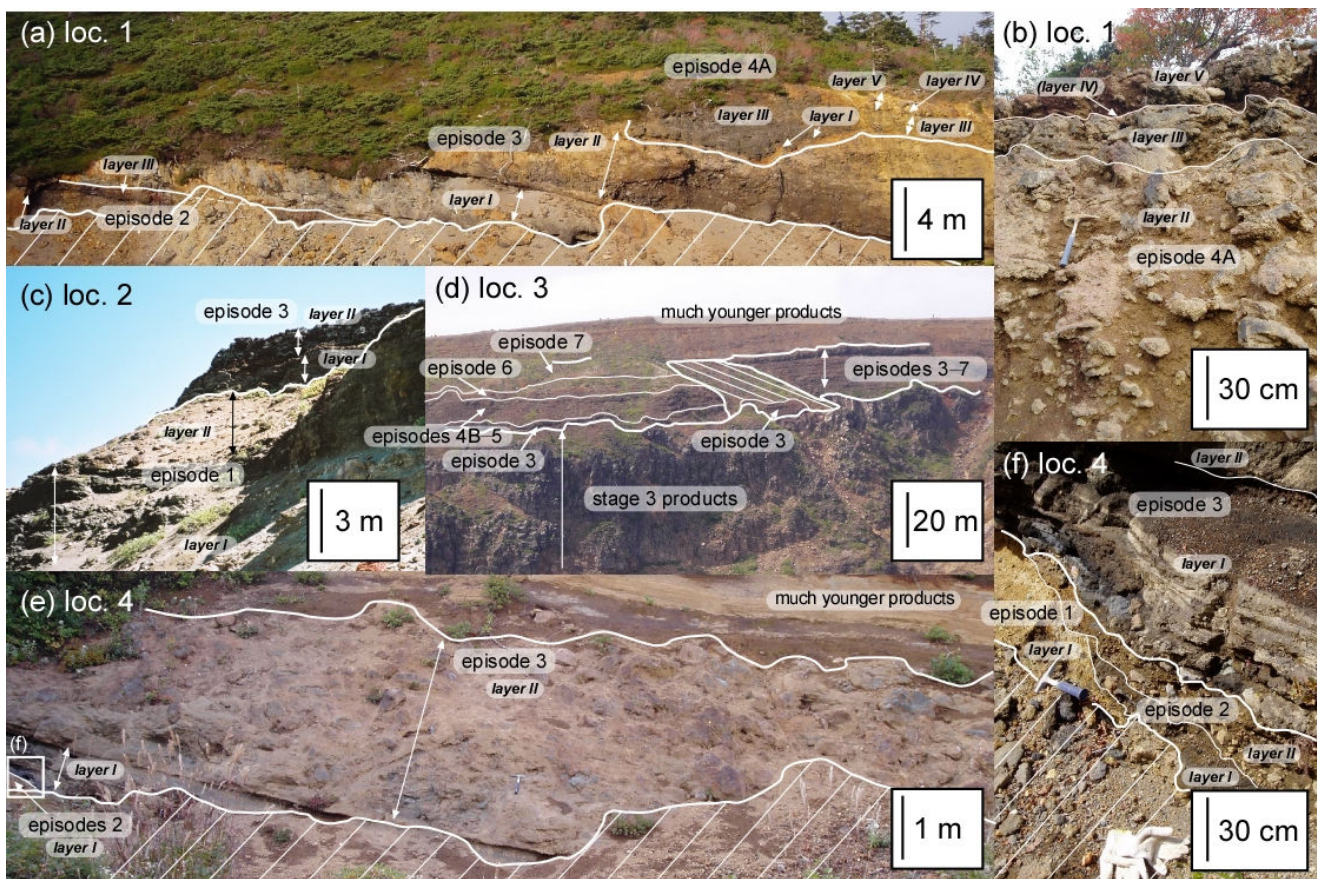


Fig. 3 Photographs of the well exposed outcrops for the Komakusadaira pyroclastics. The areas with white slash lines in some photographs indicate ones where the products are covered by colluvium. (a) A photograph of the outcrop at loc. 1 in south part of the caldera rim. (b) A photograph of the upper part (episode 4A) of the outcrop at loc. 1. (c) A photograph of the outcrop at loc. 2 in south part of the caldera rim. (d) A photograph of the outcrop at loc. 3 in the caldera rim. (e) A photograph of the outcrop at loc. 4 in southeastern part of the caldera rim. (f) A photograph of the lower part of the outcrop at loc. 4.

episode 1 products are consisted of two sets of pyroclastic layers (I and II). Both pyroclastic sets are represented by lower tuff breccia and upper scoriaceous tuff facies (Fig. 4n). Boundaries between these facieses are obscure. The thicknesses

of tuff breccia facies of layer I is ca. 7 m, while that of layer II is ca. 2 m. The thicknesses of scoriaceous tuff facies of layers I and II is ca. 2 m. Minor amount of juvenile materials are observed in deposits except for tuff breccia belong to layer II.



Fig. 4 Photographs of representative geologic features for five facies. (a) to (e) showing scoriaceous tuff facies. (a) Scoria fragment in scoriaceous tuff layer (episode 3, layer I). (b) An andesitic bomb in scoriaceous tuff layer (episode 4B, layer I). (c) A photograph of the typical layer of scoriaceous tuff facies (episode 3, layer I). The layers show the planar or cross stratified bed. (d) A layer consisted of reddish scoriaceous ash, showing dune structure. Altered lithics are observed in the part showing the dune structure (episode 3, layer I). (e) Deformed lapilli-rich lenses in scoriaceous tuff layer (episode 3, layer I). (f) and (g) showing lapilli tuff facies (layer I of episode 5 and layer II of episode 6). The areas of slash lines in photographs indicate surface or colluvium. The hammer is ca. 25 cm in length.

The episode 1 products are overlain directly by brown loam at this locality (Fig. 2). Only the tuff breccia facies of layer I is exposed at the loc.1 and 4. At both localities, the tuff breccia facies of layer I is covered unconformity by episode 2 products with erosional surface.

B. episode 2

The episode 2 products were observed at locations 1 and 4 (Fig. 1). The best exposure of episode 2 products is at an outcropping at location 1 (Fig. 3a, e and f), where episode 2 products are of three layers (I–III, Fig. 2). Layer I is ca. 1 m

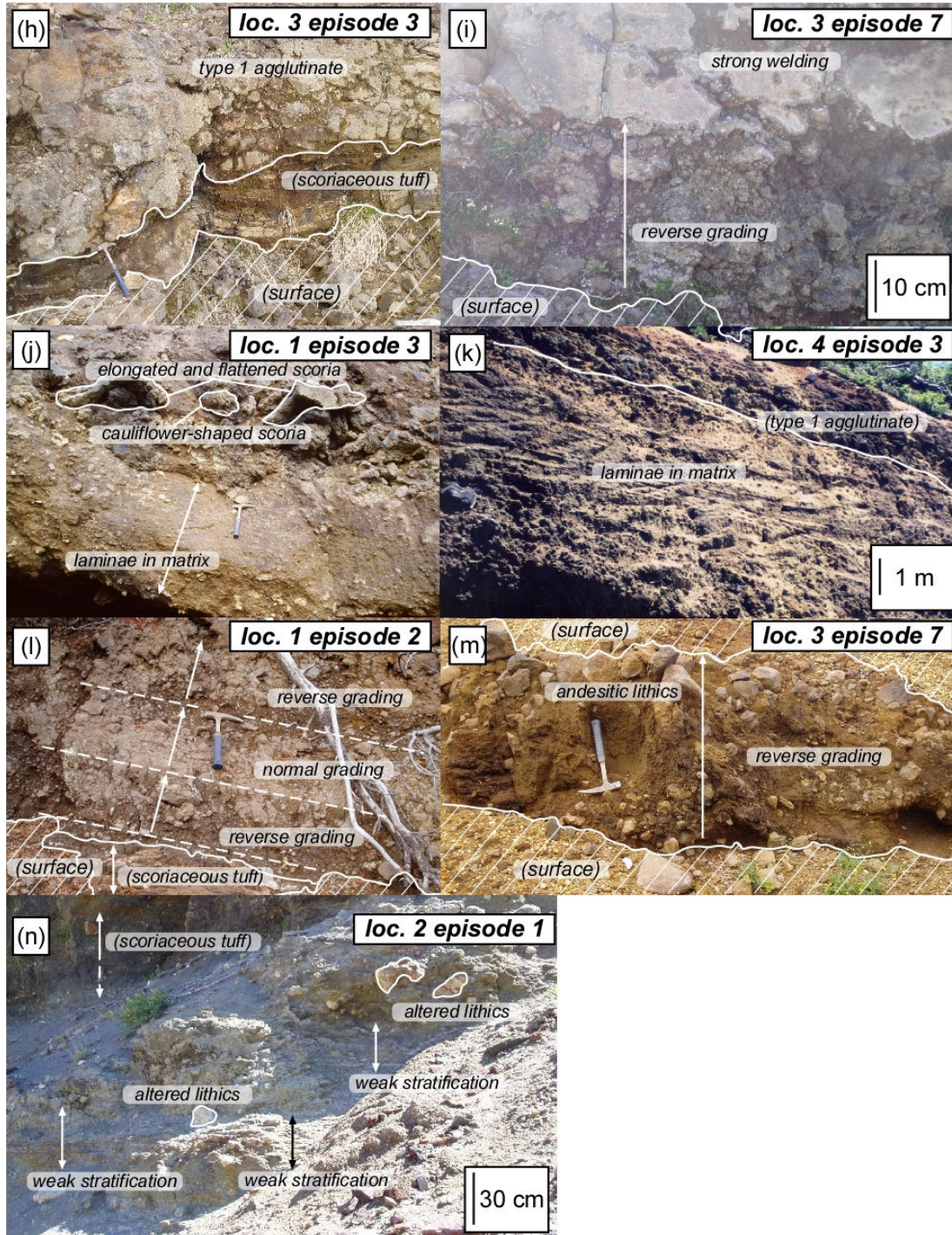


Fig. 4 continued. (h) showing overview of type 1 agglutinate facies (layer II of episode 3). (i) showing reverse grading and welding of type 1 agglutinate facies (layer III of episode 7). (j) showing type 2 agglutinate facies. (k) showing laminae in matrix (layer II of episode 3). (l) and (m) showing volcanic breccia facies (layer II of episode 2 and layer I of episode 7). The areas with slash lines in photographs indicate the surface or colluviums. The hammer is ca. 25 cm in length

thick, represented by alternation of beds of scoriaceous tuff, lapilli tuff, and reddish tuff breccia facies. Thickness of individual beds is ca. 2–15 cm. Minor amounts of juvenile lithics (up to 1 cm) are observed in the lapilli tuff bed. Layer II is ca. 5 m thick of volcanic breccia facies. In the lower part (within 2 m thickness from the base of middle layer II), reverse and normal grading of 30–50 cm intervals are repeatedly observed (Fig. 4l). In contrast, the middle (within 1.5 m thickness from the lower part of layer II) and upper (within 1.5 m thickness upward from the middle part of layer II) parts are ungraded. Scoria fragments are found sparsely in lower and upper parts; they are absent in the middle part. In the upper part, the percentage of scoria fragments increases toward upward. Layer II is covered by ca. 1 m thick layer III, showing reddish type 1 agglutinate facies. The boundary separating layer II from layer III is gradual. Layer III shows reverse grading within ca. 10 cm from the base and ca. 30 cm from the top.

The Scoriaceous tuff facies of layer I (up to 5 cm) and volcanic breccia facies of layer II (up to 10 cm) are also found at location 4. At this outcrop, type 1 agglutinate facies is absent. In both of locations 1 and 4, the volcanic breccia facies of layer II is unconformity overlain by episode 3 products.

C. episode 3

The episode 3 products are distributed mainly on the southern to eastern part of top of the caldera rim, but also on the western and northeastern part. They show up to 11 m thick pyroclastic succession. The best exposure of episode 3 products crops out at location 1 (Figs. 1 and 3). At this outcrop, the deposits are divisible into two layers (I and II, Fig. 2). Layer I (Fig. 4a, c, d, and e) consists of ca. 4 m thick scoriaceous tuff facies deposits. The lower part (within 2 m thickness from the base of layer I) and upper part (within 1.5 m thickness from the top of layer I) comprise a planar to cross-stratified bed. The middle part (within 1.5 m thickness from the lower part of layer I) is massive to cross the stratified bed poorly. Lapilli-rich lenses consisting of yellow scoriaceous lapillus are observed in the middle part. Juvenile materials (ca. 20 cm) are rarely found in the lower and upper parts. Layer I is overlain by ca. 7 m thick type 2 agglutinate facies layer (layer II, Fig. 4j), which is the thickest layer of the Komakusadaira pyroclastics, indicating that the most explosive eruptions occurred during this episode. The percentage of scoria fragments in layer II varies (Fig. 4j). At this outcrop, the contact between layer II and episode 4 products is marked by an erosion surface.

At the other three outcrops (loc. 2, 3, and 4 in Fig. 1), layer I is 50 cm to 1 m thick consisted of black and reddish scoriaceous tuff facies deposits (Fig. 4h). The facies of layer II varies on locations. At location 2 and 3, the layer II consists of strongly welded type 1 agglutinates facies (Fig. 4h). Reverse and normal grading of ca. 50 cm intervals are repeatedly observed. At location 4, the layer II shows non-welded type 2 agglutinate facies resemble to that of location 1. Thicknesses of layer II of these outcrops are ca. 2–3 m.

D. episode 4A

The episode 4 products are distributed on the southern to eastern part and western part of the caldera rim. At location 1 on

the southeastern part, the products are represented by piles of type 1 and 2 agglutinate facies deposits, whereas those at location 3 on western part consist of mainly scoriaceous tuff with thin type 1 agglutinate facies deposits. These products exposed in the southern and western parts are considered to be same stratigraphic position. The difference in facies would be because of topographic control and difference of distance from vent. Also juvenile lithics in both products have same petrological features which will be described in later chapters. Here, we describe the geologic features of the products in the southern to eastern area (deposits at loc. 1; episode 4A) and those in the western area (deposits at loc. 3; episode 4B), individually.

The episode 4A products consist of succession of type 2 agglutinate, type 1 agglutinate and scoriaceous tuff facies deposits (Figs. 2 and 3b). These deposits are 20 cm to 3 m thickness. Juvenile lithics of episode 4A products are dominantly black or oxidized reddish scoria fragments with minor amount of weakly vesiculated andesite. The scoria fragments show widely various shape; these are elongated and flattened or cauliflower-shaped at the base layer and fluidal-shaped at the top layer. Andesitic bombs are absent in lower to middle layers, and are found in two layers from the top.

E. episode 4B

The episode 4B products are divisible into three layers (I–III, Fig. 2). The thicknesses of three layers are ca. 8 m, 30 cm, and 1 m, respectively. The layers I and III show scoriaceous tuff facies (Fig. 4b). Both layers often contain juvenile scoriaceous andesitic bombs (ca. 10–30 cm in average, up to 1.5 m). The layer II is thinner, and show slightly reddish type 1 agglutinate facies.

F. episode 5

The best exposure of episode 5 to 7 products is outcropping at the location 3 on the western part of top of the caldera rim (Figs. 1 and 3d).

The episode 5 products can be divided into four layers (I–IV, Fig. 2). The thickness of the following description is that at the location 3. The basal layer I (Fig. 4f) is ca. 30 cm thick lapilli tuff facies without juvenile lithics. The layers II and IV are consist of scoriaceous tuff facies deposits layers. Minor amount of juvenile scoria fragments (up to 20 cm) are observed in these. The thicknesses of these layers are ca. 5 m and 2 m, respectively. The layer III consists of ca. 50 cm thick type 1 agglutinate facies deposits. The scoria fragments within layer III is black.

G. episode 6

Episode 6 products can be divided into three layers (I–III, Fig. 2), which is well defined at the location 3. The thicknesses of three layers are ca. 2 m, 50 cm, and 50 cm, respectively. The layer I consists of scoriaceous tuff facies deposit. Minor amount of elongated and flattened reddish scoria fragments are observed. This layer is covered by the layer II, which is consisted of lapilli tuff facies deposit (Fig. 4g). The layer III consists of orange tuff breccia.

The secondary deposit is found between products of episodes 6 and 7. Thickness is up to 5 m. This deposit is matrix supported containing subangular to subrounded, reddish to yellow andesitic grains (ca. 5–10 cm). The matrix is reddish brown ash to clay.

H. episode 7

The episode 7 products are divisible into three layers (I–III, Fig. 2), which is well defined at the location 3. The thicknesses of layers I, II and III are ca. 3, 2, and 3 m, respectively. The layer I shows volcanic breccia facies (Fig. 4m). The reverse grading by the variation of the size of blocks is remarkable. The size is up to 10 cm at the basal part (within 50 cm thickness from base of layer I), while that is up to 20 cm at the top (Fig. 4m). Scoriaceous andesite blocks are occasionally found except for basal part. The layer I is unconformity covered by the layer II show brown scoriaceous tuff facies. The layer III is type 1 agglutinate (Fig. 4i). Reverse grading of the size of reddish scoria fragments can be observed. The size is 5–15 cm in bottom and 30–50 cm in the top of the layer. The boundary of the layer II and III is not exposed.

I. Summary of geologic features of each episode

As a whole, all episodes, except for episode 7, are characterized by the domination of the facies, indicating phreato or phreatomagmatic eruptions.

Based on the detailed geologic observation of pyroclastics succession, it was revealed that the stratigraphic features are different among episodes, which is indicating that the temporal change in the mode of eruptions. The tuff breccia facies is dominated in episode 1. The juvenile fragments are minor even if they are presented. These features are suggesting that phreato to phreatomagmatic eruptions (with minor amount of juvenile fragments) have mainly occurred. In episode 2, the main facies is the volcanic breccia, which is suggesting the vulcanian was the main type of eruption. Earlier part of the episode 3 is characterized by the scoriaceous tuff facies, while the later part is by the type 2 agglutinate facies. Thus phreatomagmatic eruptions are thought to be the main type of eruption, but in the later part, abundant spatter and ballistic bombs were emitted simultaneously with the formation of pyroclastic surge. In episode 4, the type 2 agglutinate and the scoriaceous tuff facies are the main facies with subordinate type 1 agglutinate facies. Thus the eruption mode would be similar to that in the later part of episode 3, but the explosivity of activity would be decreased judging from higher percentage of the scoriaceous tuff facies. In episodes 5 to 7, the scoriaceous tuff facies with minor amounts of scoria fragments is dominant. The explosivity of activity would be further decreased from preceding episode.

V. PETROGRAPHY

We collected more than 100 juvenile rocks from the Komakusadaira pyroclastics. Phenocryst assemblages of rocks from each episode are summarized in Table 1. Rocks of episodes 1–4 are olv-bearing cpx-opx basaltic andesite to andesite, whereas those of episodes 5–7 are olv-cpx-opx basaltic andesite to andesite. The volume of total phenocrysts is

17–35%. The basaltic groundmass [10], composed of acicular shaped plagioclase microlites (up to 0.3 cm across) with Table 1 Phenocrysts assemblage for each episode of the Komakusadaira pyroclastics

Table 1 The modal composition for each episode of the Komakusadaira pyroclastics

	Episode						
	1	2	3	4	5	6	7
Total phenocryst (vol%)	24.1-35.3	17.5-21.3	17.0-29.9	17.9-30.6	16.5-20.7	23.2-34.2	16.9-27.4
Plagioclase (vol%)							
Total	13.3-25.6	11.8-17.1	12.4-20.5	12.6-23.9	10.9-17.1	15.2-22.2	12.3-18.7
Honeycomb	0.5- 4.7	6.8-12.2	6.1-11.9	10.4-11.1	4.0- 9.6	2.1- 7.3	1.7-13.0
Patchy	7.2-10.2	1.5- 4.2	4.4- 7.0	4.8- 7.0	3.8- 5.8	5.2- 5.4	2.1- 9.5
Oscillatory	2.6-20.8	0.9- 4.2	1.0- 5.5	1.0- 7.4	1.1- 9.5	5.5- 6.8	1.0- 7.9
Clear	<0.9	<0.7	<0.9	<0.8	<3.1	<0.5	<1.3
Orthopyroxene (vol%)	6.5-9.5	3.6-4.8	4.0-6.4	3.6-8.1	2.4-4.6	5.8-8.0	2.7-6.5
type 1	○	○	○	○	○	○	○
type 2	—	—	—	—	—	—	—
type 3	○	—	—	—	—	—	○
Clinopyroxene (vol%)	0.6-4.7	0.1-2.5	0.6-3.1	0.3-4.6	0.3-2.1	1.4-3.5	0.5-5.4
type 1	○	—	○	○	○	○	○
type 2	—	○	○	○	—	—	—
Olivine (vol%)	<0.3	tr.	tr.	tr.	0.3-2.8	<1.0	<3.6
type 1	○	—	○	○	○	○	○
type 2	—	○	—	—	○	—	○
Fe-Ti oxides (vol%)	<0.25	<0.10	<0.25	<0.25	<0.40	<0.45	<0.35

> 2000 points were counted for analyses; ○, detected; —, non detected; tr. < 0.1 vol%;

interstitial glass and bubbles, is sometimes observed in rocks of episode 7. Olivine phenocrysts exist in the central part of the basaltic groundmass.

A. Olivine

Fig. 5 shows the photomicroscope images (Fig. 5a) and sketches (Fig. 5b) of each textural type for phenocrystic mafic minerals. Olivine phenocrysts (up to 0.6 cm) except for those in the basaltic groundmass are classified into the following two textural types. Type 1 is euhedral to subhedral; type 2 is anhedral (Fig. 5). The olivine phenocrysts are mostly categorized to type 1. Type 2 is rarely present in episodes 2, 5, and 7 (Table 1). The volume of olivine phenocryst is up to 3.6%, except for rocks of episodes 1–4 in which it is less than 0.3% (Table 1).

Type 1 sometimes shows a skeletal texture. The type 1 olivine phenocryst often includes Cr-spinel inclusions (ca. 10–40 μm) in the core, but type 2 is spinel inclusion free. Some type 1 in episodes 4B and 6 have a 20–50 μm thick mantle part surrounding the core. Type 1 generally has no reaction rim, except for some grains having thin reaction rims of pigeonites. All type 2 phenocrysts have reaction rims. These are thick (ca. 50–200 μm); they consist of orthopyroxenes and symplectic Fe-Ti oxides (Fig. 5). The olivine phenocrysts in the basaltic groundmass, observed only in episode 7, resemble those of Type 1, but have no spinel-inclusion. Olivine phenocrysts without the reaction rims have the overgrowth of thin rim.

B. Clinopyroxene

Clinopyroxene phenocrysts (up to 0.8 cm) are divided into two textural types (Fig. 5). The type 1 is observed in all episodes except for episode 2, whereas type 2 is from episodes 2–4. Type 1 is euhedral to subhedral, in contrast type 2 is anhedral (episode 2) or euhedral to subhedral (episodes 3–4) (Fig. 5 and Table 1). The clinopyroxene phenocryst volume is up to 5.4% (Table 1).

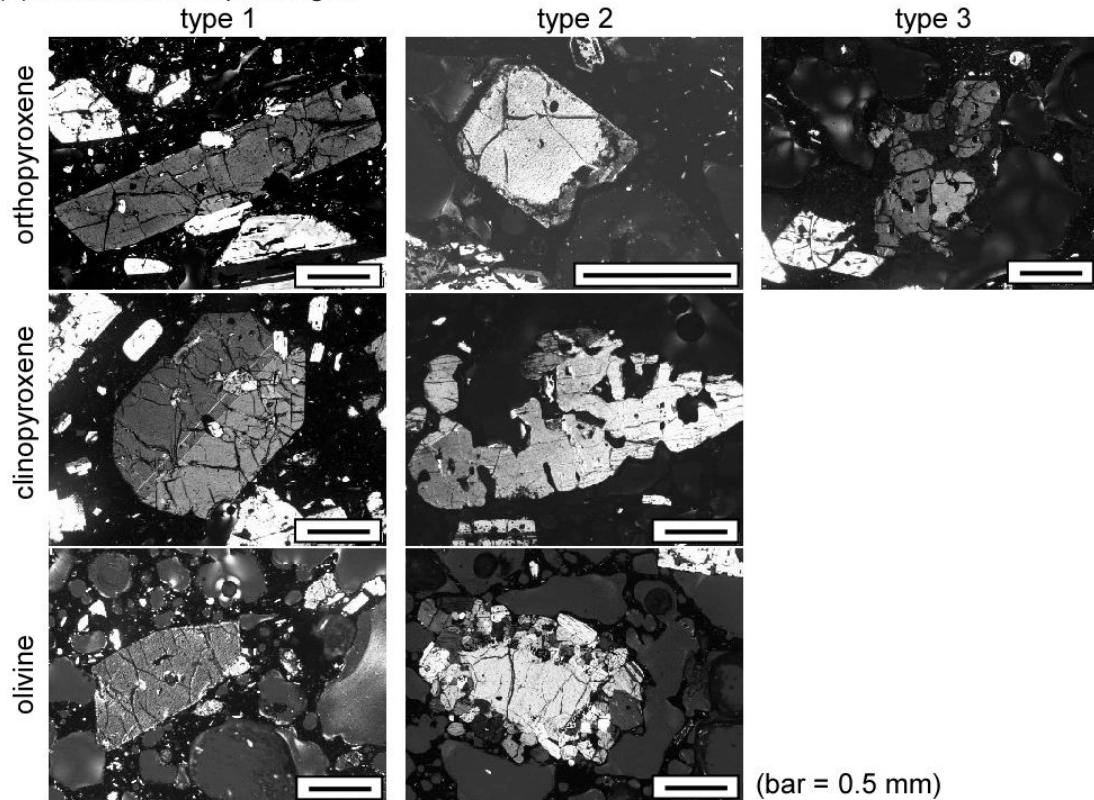
Both types contain many glass inclusions (up to 300 μm). Small sized glass inclusions (up to 10 μm) sometimes constituting dusty zones. Both types often include tiny plagioclase and Fe-Ti oxides crystals. All type 2 phenocrysts show a patchy zoned core (Fig. 5). Usually, type 1 shows no zoning, although some show it in the part (rim) within less than 100 μm from the margin. Type 2 from episode 2 shows embayed shaped and shows no zoning, whereas those from episodes 3–4

show a zoning of up to 100 μm thickness (rim) from the margin.

C. Orthopyroxene

Orthopyroxene phenocrysts (up to 0.7 cm) are classified into the following three textural types (Fig. 5). Type 1 is observed in all episodes, whereas types 2 and 3 are from episode 4, and from episodes 1 and 7, respectively (Table 1). The orthopyroxene phenocryst volume is ca. 2.4–9.5% (Table 1).

(a) Photomicroscope images



(b) Sketches of representative phenocrysts

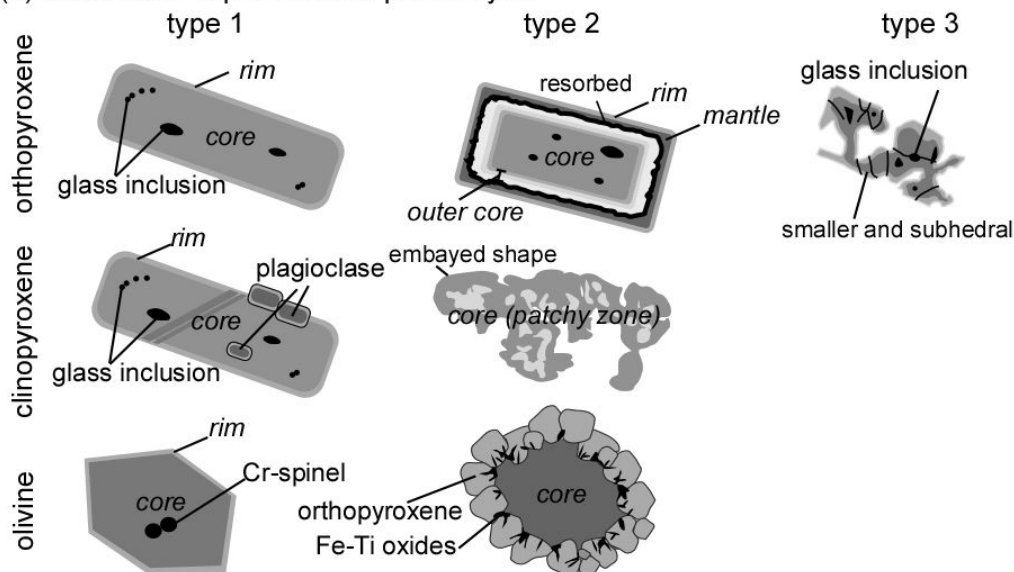


Fig. 5 (a) Photomicroscope images of textural types for phenocrystic mafic minerals. (b) Sketches of representative types for phenocrystic mafic minerals. See text for the detailed explanation.

Type 1 and 2 phenocrysts are euhedral to subhedral. Circular or irregularly shaped glass inclusions (up to 100 μm) are commonly observed, sometimes constituting dusty zones. In the case of type 1, the overgrowth rim with the width of less than 100 μm is usually observed, but some from episodes 2, 5, 6, and 7 have no such rim. Overgrowth of clinopyroxene or parallel intergrowth with clinopyroxene (up to 50 μm width) is often observed in all episodes. Type 2 has a core that is identical to that of normal zoned crystal of type 1, but the gradual zoned part is 50–100 μm thick (outer core). In addition, surrounding the outer core, a mantle part of less than 50 μm width is observed. The outline of the outer core shows a resorbed texture. The mantle part is farther overgrown by thin rim.

Type 3 orthopyroxene phenocryst is subhedral and smaller (Fig. 5). Most type 3 phenocryst cores contain tubular or irregularly shaped glass inclusions (less than 50 μm). All type 3 phenocrysts have a zoned rim within 50 μm thickness.

D. Plagioclase

Plagioclase phenocrysts (up to 0.8 cm) are divided into four textural types: honeycomb texture [11], oscillatory zoning, patchy zoning [12] and clear types. Fig. 6 shows the photomicroscope images (Fig. 6a) and sketches (Fig. 6b) of each textural type for plagioclase phenocrysts. The total volume of plagioclase phenocryst is ca. 10.9–25.6% (Table 1). The phenocrysts in episode 1 are mostly patchy zoning and oscillatory zoning types. In contrast, most plagioclases in episodes 2–4 are honeycomb type. Especially, as much as 80% of the plagioclase in episode 2 is of honeycomb type; that percentage decreases toward episode 4 (ca. 60%). In episodes 5–7, the respective relative abundances of honeycomb texture, oscillatory zoning, and patchy zoning type phenocrysts are ca. 30, 30, and 40%. The clear type is rare, but it is found in every rock.

The honeycomb texture type (Fig. 6) is mostly euhedral to subhedral. Most of this type contains irregularly shaped large (up to 300 μm) glass inclusions, but some of this type in episodes 5, 6, and 7 contain smaller glass inclusions (Fig. 6). The glass inclusions are often mutually connected by narrow channels. Each glass inclusion contains up to ca. 10 bubbles. The bubble diameters are usually less than several micrometers, although some are more than 100 μm . In episode 4, most of the parts of the glasses are replaced by plagioclase crystals that are connected with the rims (Fig. 6). Rounded clinopyroxene (augite) inclusions are sometimes observed in core. Anhedral pigeonite inclusions are occasionally observed in the cores of the phenocrysts that have smaller glass inclusions.

The oscillatory zoning type (Fig. 6) has an oscillatory zoned core. The degree of oscillation varies. The core outline shows an irregular and rounded surface surrounded by the dusty zone [13]. The outermost part is the overgrowth of the clear thin rim.

The patchy zoning type (Fig. 6) has a moderate amount of circular to irregularly shaped glass inclusions and An-poor parts (up to 300 μm), which constitute patches in oscillatory zoned core. The core is surrounded by oscillatory zoned mantle (50 μm to 1 mm wide) and is further surrounded by a clear thin rim. A thin dusty zone identified by fine glass inclusions (diameter of 20 μm or less) is sometimes observed in the mantle.

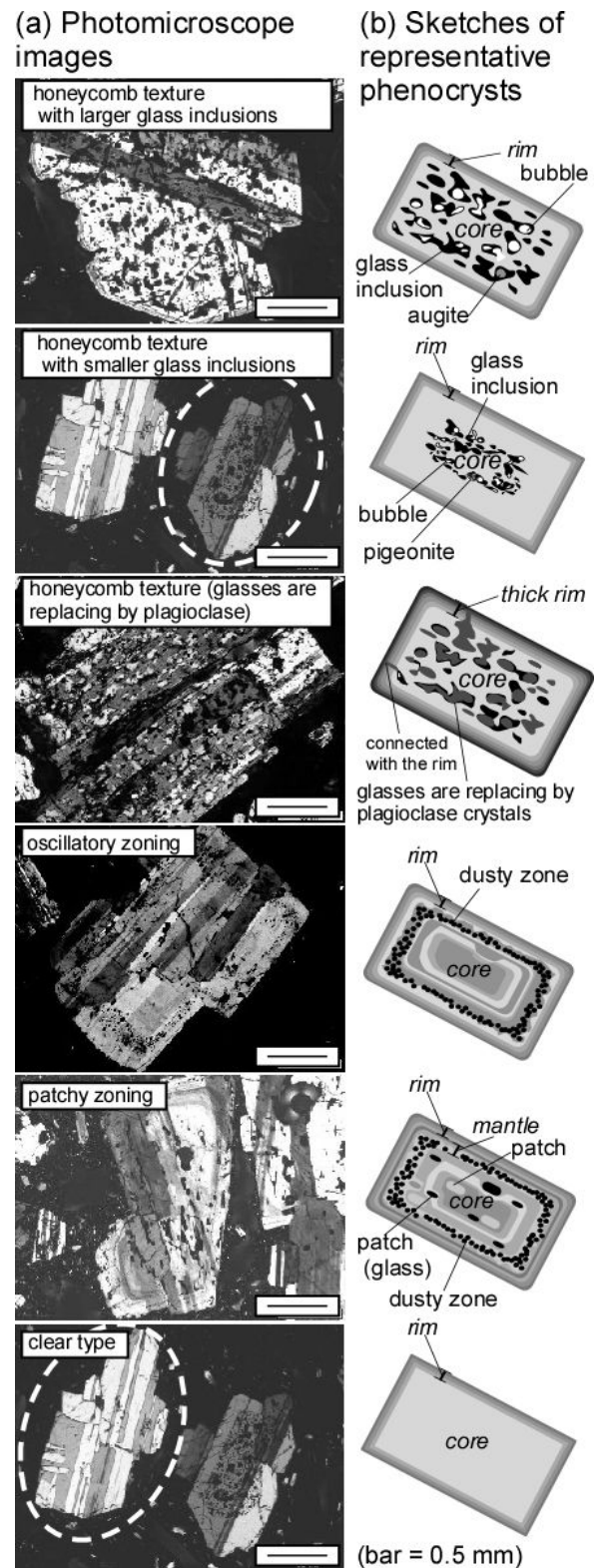


Fig. 6 (a) Photomicroscope images of textural types for plagioclase phenocrysts. (b) Sketches of representative types for phenocrysts. See text for the detailed explanation.

The clear type (Fig. 6) is euhedral. This type always has a clear core. The cores of this type are often surrounded by mantle (less than 500 μm wide), which shows similar texture to that of an oscillatory or patchy zoning type.

The rims of plagioclase phenocryst generally appear to be homogeneous, but when examined carefully, weak oscillatory zoning is visible. The rim thickness varies. The rims of the honeycomb texture type, except in episodes 3 and 4, are as thick as 20 μm , although those of honeycomb type in episodes 3 and 4 are thicker (as thick as 50 μm). The rims of patchy and oscillatory zoning types are ca. 20 μm thick. The rims of clear type are thinner (less than 10 μm). The rim of the clear type is distinguished from the core by differences in the extinction angles.

E. Fe-Ti oxides

Fe-Ti oxides (up to 0.1 cm) are mostly subhedral, whereas some Fe-Ti oxides show equant-shaped. The Fe-Ti oxides phenocryst volume is less than 0.5%.

VI. CORRELATION OF THE KOMAKUSADAIRA PYROCLASTICS TO DISTAL TEPHRA LAYERS OF THE ZAO VOLCANO

The tephra layers of the newest activity of Zao volcano are distributed in summit area to eastern foot of the volcano. The tephrostratigraphic studies for those tephra layers were performed by various authors [7], [14] and [15]. Sixteen black scoriaceous tuff layers (Z-To 1–4, 5a, 5b, 6–14 in ascending order) were recognized by [16]. The Komakusadaira agglutinate is correlated to the older four tephra layers (Z-To 1 to 4) [7]. Reference [7] reported the ages and volumes of Z-To 1–4 layers distributed around the eastern foot of the Zao volcano. The ages of four tephra layers are ca. 33–32, 30.7, 27.1 and 12.9 kyr BP [7]. Z-To 1 layer occurs as lenses, while the other three layers present as stratified layer in outcrop of eastern foot of Zao [7]. Z-To 2 layer is the thickest among these. This layer is divided into three parts, lower, middle and upper [7]. The lower and upper parts are composed of black scoriaceous tuff, whereas middle part is mainly composed of reddish oxidized and lapilli sized scoria fragments. This reddish scoria part is the Zao Kawasaki scoria named by [15].

As described in the chapter of stratigraphy, the episode 3 products show up to 11 m thick pyroclastic succession indicating that the most explosive eruptions occurred during episode 3. Especially, layer II of the episode 3, which is thickest layer throughout the newest activity, contains abundant spatter and ballistic bombs. We infer that the layer II of episode 3 correlates to the Zao Kawasaki scoria. The products of episodes 2 and 4 are bounded from episode 3 products by unconformities. These surfaces of unconformity would be caused by erosion of overlying surge deposits, and would not show long time gap (loc. 1 and 4; Fig. 2). Consequently, the products of episodes 2 and 4 correlated to lower and upper parts of Z-To 2 layer. In contrast, a brown loam layer intercalates to the products of episodes 1 and 2. The basal layer of episode 5 products is lapilli tuff facies without juvenile lithics, which would suggest the beginning of a brand-new activity. Thus, it is probable that the

time gaps between episodes 1 and 2, and episodes 4 and 5 would be longer. From above consideration, the products of the episodes 1 and 5–7 is deduced to be correlated to layers of Z-To 1 and 3, respectively.

VII. TEMPORAL CHANGE OF STRATIGRAPHIC AND PETROGRAPHIC FEATURES OF THE KOMAKUSADAIRA PYROCLASTICS

As deduced in the previous chapter, the activity of the Komakusadaira pyroclastics can be divided into three periods; episodes 1, 2–4, and 5–7. The tuff breccia facies is dominated in episode 1. The products of episodes 1 to 4 are mainly deposited at south to eastern part, and thus the crater of episodes 1–4 products would be located in south part of the present crater lake Okama in the Umanose caldera. Furthermore, the pyroclastic surge usually travels downhill whereas the episodes 1–4 products are observed at higher rims of caldera. We therefore infer that the altitude of the crater during the activity of the episode 1–4 is higher than the one of the present crater lake Okama. Fig. 7 indicates the schematic images of the eruptions of representative parts of episodes 1 and 3. The phreatic to phreatomagmatic with minor amount of magma eruption would be occurred repeatedly in the period of episode 1 (Fig. 7a). In the period of episodes 2–4, the eruption type had changed from the vulcanian in the early part to the phreatomagmatic with abundant spatter and ballistic bombs in the middle part (Fig. 7b). The phreatomagmatic eruptions would be continued to the late part but the explosivity would be decreased. In the period of episodes 5–7, the type of the eruption is mainly the phreatomagmatic. The explosivity of activity would be much smaller than that of the former period.

The petrographic features are different among three periods; episodes 1, 2–4, and 5–7. Phenocrysts of mafic minerals are mostly of type 1 and plagioclase phenocrysts are mainly patchy or oscillatory zoning type in the period of episode 1. In contrast, type 2 orthopyroxene and clinopyroxene, and honeycomb texture plagioclase with larger glass inclusions are remarkably observed in the period of episodes 2–4. In the period of episodes 5–7, type 2 as well as type 1 olivine phenocrysts and honeycomb texture plagioclase with smaller glass inclusions characteristically participate in the assemblage.

As described above, episodes 1, 2–4, and 5–7 have identical characteristics in stratigraphy and petrography. Also, age gaps between activities of these three periods are inferred as in discussed in the previous chapter. These contrasting features would be suggesting that distinct magma feeding systems had been operated for these three periods. The petrologic consideration of the magma feeding system will be presented in the other article

VIII. CONCLUSION

We obtained detailed stratigraphic and petrographic data on the Komakusadaira pyroclastics of the Zao volcano in northeastern Japan. These data will be one of representative examples on temporal change of geologic and petrographic

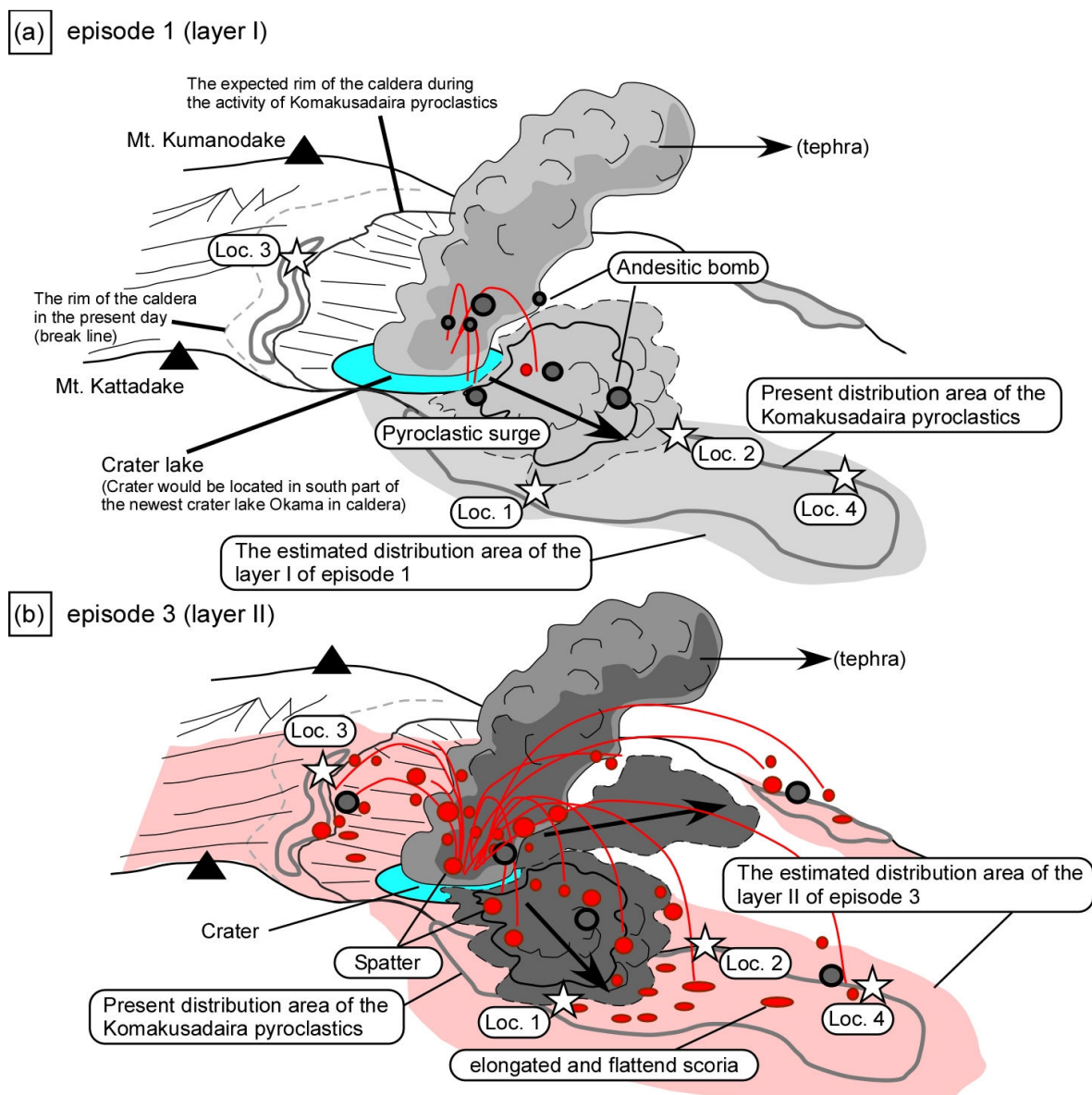


Fig. 7 Schematic images of the eruptions of episodes 1 and 3 of the summit area of Zao volcano. (a) Schematic image of the phreatomagmatic eruption of the layer I of episode 1 activity. (b) Schematic image of the phreatomagmatic with abundant spatter and ballistic bombs of the layer II of episode 3 activity

features of the pyroclastic surge dominated surge deposits of the stratovolcano with crater lakes. These data will also be fundamentally useful information to elucidate future volcanic activity.

The activity is divided into seven episodes (episodes 1–7), which is further grouped to three periods (episodes 1, 2–4, and 5–7). The ages of these three periods are estimated to be ca. 32–33, 31, 27 kyr BP. The pyroclastics are formed in 27 layers by scoriaceous tuff, lapilli tuff, agglutinate, volcanic breccia, and tuff breccia. The agglutinate facies is divided into two types. One is fall origin and the other is formed by associating with pyroclastic surge. The three periods of episode 1, episodes 2–4 and episodes 5–7 are characterized by the facieses of tuff breccia, volcanic breccia–second type agglutinate, and

scoriaceous tuff, respectively.

The phreatic to phreatomagmatic with minor amount of magma eruption would be occurred repeatedly in the first period. During the second period, the eruption type had changed from the vulcanian to the phreatomagmatic. By the phreatomagmatic eruptions, pyroclastic surges with abundant spatter and ballistic bombs had occurred. The phreatomagmatic eruptions would continue to the late part of this period but the explosivity would decrease. In the third period, the type of the eruption is mainly the phreatomagmatic, but the explosivity of the activity would be much smaller than that of the former period. Consequently, the crater lakes would have been intermittently formed and sometimes disappeared at the summit area during the activity of the Komakusadaira pyroclastics.

The petrographic features are different among the three periods. The period of the episode 1 is characterized by mafic minerals of mostly type 1 and plagioclases are mainly patchy or oscillatory zoning type in. While in the period of episodes 2–4, type 2 orthopyroxene and clinopyroxene, and honeycomb texture plagioclase with larger glass inclusions are remarkable. In the period of the episodes 5–7, olivine phenocrysts are abundant and honeycomb texture plagioclase with smaller glass inclusions observed characteristically. These differences would reflect those of the magma feeding systems.

Submitted by

Masao Ban
Department of Earth and Environmental Sciences,
Faculty of Science, Yamagata Univ.,
Yamagata, 990-8560, Japan
ban@sci.kj.yamagata-u.ac.jp

Yoshinori Takebe
Department of Earth and Environmental Sciences,
Faculty of Science, Yamagata Univ.,
Yamagata, 990-8560, Japan
s07e104d@st.yamagata-u.ac.jp

ACKNOWLEDGMENT

We are grateful to Drs. K. Nakashima, K. Saito, S. Hirotsu, and K. Miura for constructive comments on this research.

REFERENCES

- [1] R.F.A. Cas, and J. V. Wright, “*Volcanic Successions: A Geological Approach to Processes, Products, and Succession*, In Allen and Unwin (eds),” London, pp. 528, 1987.
- [2] J.B. Shepherd, and H. Sigurdsson, “Mechanism of the 1979 explosive eruption of Soufriere volcano, St. Vincent,” *J. Volcanol. Geotherm. Res.*, vol. 13, pp. 119–130, 1982.
- [3] G. Kilgour, V. Manville, F. Della Pasqua, A. Graettinger, K.A. Hodgson, and G.E. Jolly, “The 25 September 2007 eruption of Mount Ruapehu, New Zealand: Directed ballistics, surtseyan jets, and ice-slurry lahars,” *J. Volcanol. Geotherm. Res.*, vol. 191, pp. 1–14, 2010.
- [4] N. Takaoka, K. Konno, Y. Oba, and T. Konta, “K-Ar datings of lavas from Zao volcano, north-eastern Japan,” *J. Geol. Soc. Japan*, vol. 95, pp. 157–170, 1989. (in Japanese with English abstract)
- [5] A. Sakayori, “Geology and petrology of Zao volcano,” *J. Miner. Petrol. Econ. Geol.*, vol. 87, pp. 433–444, 1992. (in Japanese with English abstract)
- [6] M. Ban, H. Sagawa, K. Miura, and S. Hirotsu, “Evidence for a short lived stratified magma chamber: petrology of the Z-To 5 tephra layer (c. 5.8ka) at Zao volcano, NE Japan. In: Annen C, Zellmer GF (eds) *Dynamics of crustal magma transfer, storage and differentiation*,” Geological Society, London, Special Publications, vol. 304, pp. 149–168 2008.
- [7] K. Miura, M. Ban, and H. Yagi, “The tephra layers distributed around the eastern foot of the Zao volcano –ages and volumes of Za-To 1 to 4 tephra-,” *Bull. Volcanol. Soc. Japan*, vol. 53, pp. 151–157, 2008.
- [8] Y. K. Sohn, and S. K. Chough, “Depositional processes of the Suwolbong tuff ring, Cheju Island, (Korea),” *Sedimentology*, vol. 36, pp. 837–855, 1989.
- [9] S. K. Chough, and Y. K. Sohn, “Depositional mechanics and sequence of base surges, Songaksan tuff ring, Cheju Island, Korea,” *Sedimentology*, vol. 37, pp. 1115–1135, 1990.
- [10] M. Sakuyama, “Evidence of magma mixing: petrological study of Shirouma-Oike calc-alkaline andesite volcano, Japan,” *J. Volcanol. Geotherm. Res.*, vol. 5, pp. 179–208, 1979.
- [11] H. Kuno, “Petrology of Hakone volcano and the adjacent areas, Japan.” *Bull. Geol. Soc. Am.*, vol. 61, pp. 957–1020, 1950.
- [12] J. A. Vance, “Zoning in plagioclase: Patchy zoning,” *J. Petrol.*, vol. 73, pp. 636–651, 1965.
- [13] A. Tsuchiyama, “Dissolution kinetics of plagioclase in the melt of the system diopside-albite-anorthite, and origin of dusty plagioclase in andesites,” *Contrib. Mineral. Petrol.*, vol. 89, pp. 1–16, 1985.
- [14] R. Imura, “Zao volcano. In: Takahashi M, Kobayashi T (eds) *Field guide of volcanoes in Japan 4 Volcanoes in Tohoku districts*,” Tsukiji press, Tokyo, pp. 77–88, 1999. (in Japanese)
- [15] N. Itagaki, M. Toyoshima, and T. Terado, “The scoria bed of late pleistocene in Sendai and its environs,” *Tohoku Geography*, vol. 31, pp. 48–53, 1981. (in Japanese).
- [16] M. Ban, H. Sagawa, K. Miura, and Y. Tanaka, “Hazard map of the Zao volcano,” *Chikyū monthly*, vol. 27, pp. 317–320, 2005 (in Japanese).